

## Probing the oscillating Belousov-Zhabotinskii reaction with micrometer-sized electrodes: the effect of C, Pt, and Au

Manuel A. Gracia-Nava<sup>1</sup>, Lucien Veleva<sup>1,\*</sup>, Gabriel Perez<sup>1</sup> and Mario A. Alpuche-Avilés<sup>2</sup>

<sup>1</sup> Applied Physics Department, CINVESTAV-IPN Merida, Ant. a Progreso Km.6, 97310 Merida, Yucatan, Mexico,

<sup>2</sup> Department of Chemistry, University of Nevada, Reno, Nevada, 89557-0216 USA.

\*E-mail: [veleva@mda.cinvestav.mx](mailto:veleva@mda.cinvestav.mx)

Received: 6 March 2019 / Accepted: 28 April 2019 / Published: 30 June 2019

---

The Belousov-Zhabotinskii (BZ) oscillating reaction mixture (malonic acid, bromate, and cerium ions in a strongly acidic medium) was studied. The oxidation state of the  $\text{Ce}^{+4}/\text{Ce}^{+3}$  catalyst fluctuates and drives the open-circuit potential (OCP) of the solution. Oscillatory profiles were analyzed using Au, Pt and C micro- and macro-electrodes to study the stages of induction, oscillating, and equilibrium. The oscillating behavior of the BZ system is transient, reaching a non-oscillating reductive steady-state. The time for achieving the oscillating state depends on the substrate (electrode material and size) while the number of oscillations is independent of substrate. Fast Fourier transform (FFT) analysis yields the fundamental frequency of the oscillating profile and evaluates the exponential falloff as the system approaches equilibrium. Also,  $\text{Ce}^{+4}$  concentration was tracked in the UV Vis. Chemical oscillations of the catalyst  $\text{Ce}^{+4}$  ion were reproduced using a numerical model, and its dynamical profile was analogous to the experimental data.

---

**Keywords:** BZ reaction; dissipative structure; oscillating reaction; ultra micro-electrodes

### 1. INTRODUCTION

In recent years, the study of non-linear dynamics and chaos phenomena has received great interest in scientific disciplines, [1-3] including electrochemical systems and devices [4-8]. Chemical reactions are exemplary non-linear systems, and they have provided some of the most visually astonishing evidence, including magnificent but simpler models utilized for theoretical studies [1]. The evidence of non-linear chemical behavior is everywhere. Consider, for instance, life organisms periodical phenomena, seasonal changes in leaf color, heartbeat rhythm, menstrual periods, and pattern formation in biological and geological systems [9-10]. Oscillations are also associated with metal dissolution processes [11]. Because of their broadly ranging implications, there has been a renewed

interest in the long-time stability [12] of these systems and the details of the diffusion layer in the micrometer scale [13]. The periodicity caused by the reactions and diffusion form non-equilibrium structures in soft matter with characteristic lengths in the nanometer scale [14]. The first observation of periodical behavior in a chemical system was ascribed to Robert Boyle in the late 17<sup>th</sup> century [10]. Nevertheless, oscillating chemical reactions did not attract much attention in those early days. There was a steadfast conviction that the 2<sup>nd</sup> law of thermodynamics would not permit such type of abnormality. Perhaps the primary victim of this prejudice was Boris P. Belousov, whose attempts to publish his first observations concerning chemical oscillations in mixtures of citric acid, bromate, and cerium were completely frustrated by the minds who “knew best.” However, a new dawn in the field emerged with novel and irrefutable evidence of Belousov’s oscillations by the then-young soviet biophysicist named Anatolii Zhabotinskii [15]. He was more successful in popularizing the reaction [16] which today is known as the Belousov-Zhabotinskii reaction (BZ). The BZ reaction has played a role in non-linear chemical dynamics similar to the hydrogen atom in quantum mechanics [9]. This reaction has been recently used to demonstrate that control of the oscillation with an applied potential is possible [17] and the ensemble Au NPs in spiral patterns [18]. More recently, applications in electrodeposition [19] and analysis [20-21] have been proposed.

The BZ reaction is an example of a dissipative far-from-equilibrium system, which is an ordered state of matter occurring far from the bifurcation point where the thermodynamic branch with minimum entropy production becomes unstable [22]. The oscillations arise from the interchange of heat and matter with the environment, along with entropy dissipation by the system [23]. One necessary, but not sufficient, condition, for oscillations is that at least one autocatalytic phase must be included in the reaction scheme. The general mechanism has been described qualitatively [24-25]. The BZ reaction is the oxidation of an easily brominated organic substrate catalyzed by a metallic ion in a strongly acidic medium [25]. Three major stages are considered in the reaction scheme: (1) reactions between oxybromine species; (2) autocatalytic oxidation of a metallic ion in the presence of bromate and HBrO<sub>2</sub>; and (3) reduction reactions of the catalyst and the organic substrate coupled to bromide and CO<sub>2</sub> production [26]. A detailed analysis of the BZ reaction is complicated due to several stages and participating reactants. The model introduced by Györgyi and co-workers contains at least 80 elementary reactions and 26 species of variable concentration [25]. More recently, efforts have included finding an exact solution for the concentration wave [27]. Other studies of the BZ reaction in a batch reactor were performed that included the development of a model that allowed variations of the reactant concentrations [28]. An open-gel reactor triggered by varying the light excitation threshold for a Ru complex (ruthenium-4-4'-dimethyl-2,2'-bipyridiyl) was used to study propagating spiral waves [29], but we note that here we do not use a Ru redox couple. While the different models are of interest, we note that our analysis here is based on the time dependence of the OCP and the dependence of the oscillatory behavior with electrode materials and size down to the micrometer scale, that is, within the scale of the diffusion layer.

We are interested in the effect of the different materials used here: Au, C, and Pt, which are known to have distinct electrochemical properties. Therefore, the comparison of electrodes of the same size with different materials provides insight into the oscillations of different intermediates. We will show that the C electrode has a significantly higher voltage and frequency than the Au and Pt electrodes,

likely due to the material being sensible to an organic intermediate. Concerning the different electrode sizes, the electrodes used here cover two domains: from a few tens of micrometers to a few millimeters. While previous reports use electrodes in the millimeter to centimeter scale, we present the use of microelectrodes in open circuit measurements to increase sensitivity in space and time domains. Microelectrodes are sensitive to concentration changes across a few tens of micrometers, and because of their faster time response, they can follow changes in a shorter time scale. Our data will show that microelectrodes have different pre-oscillatory times than their macroscopic counterparts. Interestingly, only small changes in frequency with size are observed with carbon macroelectrodes displaying a higher oscillation frequency than Pt and Au. Overall, we will discuss our results with the Oregonator model of the BZ reaction.

The BZ reaction oscillations are based on the existence of two states, referred to as reduced and oxidized. These two states are available for the system to change alternately from one to the other depending on the bromide ( $\text{Br}^-$ ) concentration. The reductive state is predominant at high  $\text{Br}^-$  concentration, where the majority of Ce ions approach their reduced state,  $\text{Ce}^{+3}$ , and the general chemistry is the organic substrate's bromination with simultaneous removal of  $\text{Br}^-$  from solution [25]. The most frequently used organic substrate is malonic acid (MA). Afterward, the system changes to the oxidized state when the  $\text{Br}^-$  concentration becomes rate-limiting. This state is characterized by high values in  $\text{HBrO}_2$ ,  $\text{Ce}^{+4}$ , and organic radical concentrations. Additionally, progressive bromination of MA and the ultimate oxidation of MA to  $\text{CO}_2$  occur at this state. Bromide ion is consumed slowly to produce  $\text{BrO}_3^-$  and, when the  $\text{Br}^-$  concentration diminishes to a certain critical value, the reduced state turns unstable. Then, the autocatalytic step takes control of the reaction allowing the  $\text{Ce}^{+3}$  oxidation to  $\text{Ce}^{+4}$ , [24].

In this study, the oscillating profiles of the BZ reaction were studied at different substrate electrodes: Au, Pt, and glassy carbon, micro- and macro-electrodes surfaces, using different stirring rates. The main characteristics of the BZ reaction oscillations, such as amplitude and frequency, were analyzed. Fast Fourier Transform (FFT) was applied to know the fundamental frequencies of the oscillating profiles and evaluate the exponential falloff as the system approached thermodynamic equilibrium. As an additional technique, UV-visible spectrophotometry was used to track  $\text{Ce}^{+4}$  absorbance during the BZ reaction. Chemical oscillations of  $\text{Ce}^{+4}$  ion were reproduced using numerical integration of the *Oregonator* [30]. The oscillations dynamical profile was compared to that obtained experimentally.

## 2. EXPERIMENTAL

The solutions for studying the BZ reaction were prepared using deionized water (18 M $\Omega$ cm, Thermo purifier) along with the following reactants (all reactive grade) sustained by reported methodologies [31-32]:  $\text{H}_2\text{SO}_4$  (Pharmco-Aaper), malonic acid-MA-(Sigma-Aldrich),  $\text{KBrO}_3$  (Sigma-Aldrich) and  $\text{Ce}(\text{SO}_4)_2$  (Sigma-Aldrich). Different concentrations of each of the BZ reaction components were evaluated with the purpose of establishing the optimal quantities for keeping an adequate tracing

of the BZ reaction. The final concentrations utilized in this study were: 0.9 M H<sub>2</sub>SO<sub>4</sub>, 0.10 M MA, 0.08 M KBrO<sub>3</sub>, and 1 mM Ce(SO<sub>4</sub>)<sub>2</sub>. To recreate the BZ system, three different solutions were prepared:

*Solution A* (0.2 M MA in 0.8 M H<sub>2</sub>SO<sub>4</sub>): In a flask, 80 mL of deionized water were added to 2.081 g of malonic acid. Afterward, 4.26 mL of H<sub>2</sub>SO<sub>4</sub> (98%, v/v) were added and the volume was taken to 100 mL using deionized water. *Solution B* (0.32 M KBrO<sub>3</sub> in 0.8 M H<sub>2</sub>SO<sub>4</sub>): In a flask, 80 mL of deionized water were added to 5.344 g of KBrO<sub>3</sub>. Afterwards, 4.26 mL of H<sub>2</sub>SO<sub>4</sub> (98%, v/v) were added, and the volume was taken to 100 mL using water. *Solution C* (4 mM Ce(SO<sub>4</sub>)<sub>2</sub> in 0.8 M H<sub>2</sub>SO<sub>4</sub>): In a flask, 40 mL of deionized water were added to 66.45 mg of Ce(SO<sub>4</sub>)<sub>2</sub>. Afterward, 2.13 mL of H<sub>2</sub>SO<sub>4</sub> (98%, v/v) were added, and the volume was taken to 50 mL using deionized water. 10 mL of *Solution A* and 5 mL of *Solution B* were mixed in a 50-mL beaker containing a magnetic stirrer (2.5 cm, diameter 0.8 cm). The electrodes were placed and the stirrer plate was turned on, ensuring that the magnetic stirrer neither hit the beaker's walls or the electrodes. Next, 5 mL of *Solution C* were added and the data were collected immediately. Except for the stirring, the reaction was held undisturbed.

*Working electrodes* with disk-type geometry and different substrates were used: Pt (25 μm and 1.6 mm of diameter), Au (12.5 μm and 1.6 mm of diameter) and C (carbon fiber 25 μm, and glassy carbon –GC–3 mm of diameter). Pt micro-electrodes were manufactured in the laboratory and characterized using established methods [33]. Figure 1e is a scanning electron microscopy (SEM) image of an electrode with nominal diameter of 10 μm. The rest of the electrodes were from BASi, Inc. A reference electrode of Ag/AgCl/1 M KCl (236 mV vs. NHE) was used in all experiments (CH Instruments). Open circuit potential (OCP) profile in time was registered using an electrochemical analyzer (CH Instruments, Inc.) with a sampling frequency of  $f_s = 50$  data/s at 20 °C. Before each experiment, the working electrodes' surface were mechanically polished with 0.3-μm Alumina and cleaned in an ultrasonic bath with deionized water. The experiments were placed inside a Faraday cage in a 50-ml beaker filled to constant volume with 20 mL of solution. The stirring rate was varied magnetically from 0 to 1300 rpm. OCP oscillations for the BZ reaction were characterized by Fourier Fast Transform (FFT) with the software GNU Octave 3.2.4 (Copyright© 1998-2012 John W. Eaton) [34]. Following the methodology proposed by Baird and co-workers [35], a spectrophotometer Varian 50 Scan with a UV Vis probe was used to monitor the chemical oscillations.

### 3. RESULTS AND DISCUSSION

One of the most noteworthy characteristics of the BZ system is the oscillation of the catalysts' oxidation state, [Ce<sup>+4</sup>]/[Ce<sup>+3</sup>], which influences significantly on the OCP value of a potentiometric probe [10]. Therefore, OCP changes can be monitored using an adequate electrode with Pt being used most frequently. In a closed system, the BZ reaction exhibits typically an induction period that depends on the experimental conditions [36]. We note that in the context of oscillatory reactions, the term "closed system" is used to describe a system where the initial reactants are introduced to the reaction mixture and are not replenished during the reaction. We use the term "closed systems" in this paper in keeping with the usual nomenclature, although unfortunately, this term has been traditionally used to describe systems where gases, such as oxygen and CO<sub>2</sub>, are allowed to exchange with the surroundings. The

induction period is necessary for the synthesis of brominated compounds of MA whose primordial purpose is the  $\text{Br}^-$  regeneration [37]. Subsequently, an oscillatory regime takes place. For its establishment, the production of more  $\text{Br}^-$  is required, which can be produced from the oxybromine species reduction [25].

The BZ reaction solution's color alternates between colorless and yellow, depending on the catalyst's oxidation state, and if the system is positioned in the reduced stage (high  $\text{Ce}^{+3}$  concentration) or oxidized (high  $\text{Ce}^{4+}$  concentration) state. We observed a progressive production of  $\text{CO}_2$  bubbles due to the MA oxidation.

### 3.1. Effect of the stirring rate.

In Figure 1 we present the effect of the stirring rate (0 to 1200 rpm) on the OCP oscillations in the BZ system registered with a Pt micro-electrode ( $d = 25 \mu\text{m}$ ), as result of differences in the ionic species concentration at the electrode-electrolyte interface.

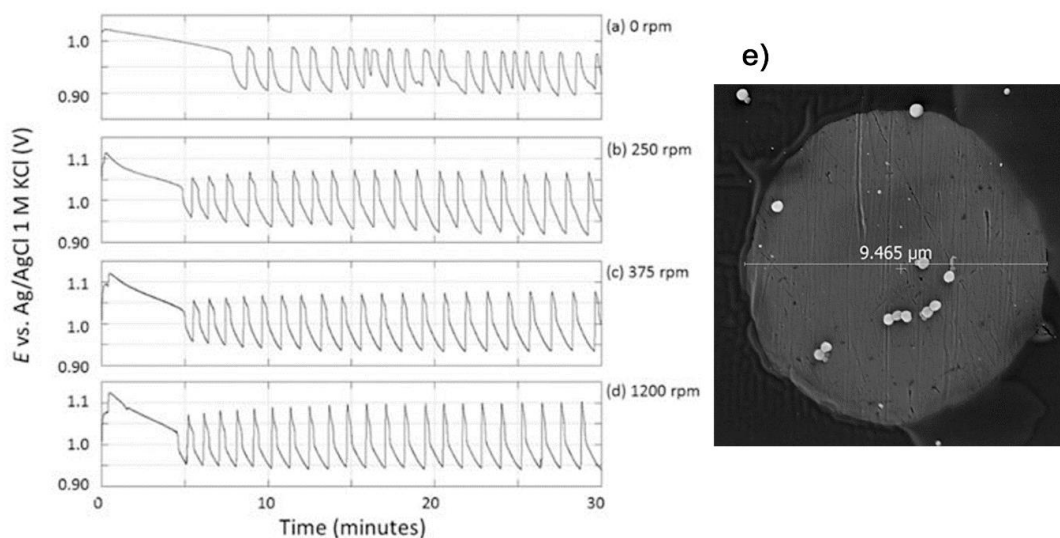


**Figure 1.** Effect of the stirring rate in the BZ system over the OCP (V) oscillations registered with a Pt micro-electrode ( $d = 25 \mu\text{m}$ ): 0.8 M  $\text{H}_2\text{SO}_4$ , 0.10 M MA, 0.08 M  $\text{KBrO}_3$ , and 1 mM  $\text{Ce}(\text{SO}_4)_2$ . (e) is an SEM image of an electrode with nominal  $d = 10 \mu\text{m}$ ; the bright spots are alumina used for polishing.

The data indicates the appearance of an induction period of several minutes before the start of the oscillating phase, in which the OCP leans towards more positive OCP values in the first seconds. After that, the OCP falls to more negative OCP values. With no stirring (0 rpm) the profile is irregular because of the  $\text{CO}_2$  bubbles adhere to the working electrode's surface. One can tell that, after introducing stirring into the system, the OCP deviates to more positive values (10 to 15 mV). Increasing stirring rates causes a reduction in the induction period, an increase in the amplitude, and a decrease in the period of

the oscillations, due to the higher mass transfer rate towards the electrode's surface. This is interesting because according to literature, the period of oscillations becomes larger as the  $\text{BrO}_3^-$  concentration reduces [24].

The oscillations show the relative simplicity of the waveforms (Figure 1), which are distinctive of periodical chemical oscillators. Period averages for the first 20 oscillations are presented, except at 0 rpm, where only the first four oscillations were used. Without stirring the fluctuations became erratic after the first 4 oscillations. The averages found are 1.273 min at 0 rpm, 1.241 min at 250 rpm, 1.204 min at 375 rpm, and 1.112 min at 1200 rpm. The corresponding amplitudes were 77 mV at 0 rpm, 140 mV at 250 rpm, 141 mV at 375 rpm, and 153 mV at 1200 rpm. Based on these results, 375 rpm was selected as stirring rate to record OCP profiles in the succeeding experiments because we observed stable profiles without causing turbulence that may affect the system. It has been reported that high stirring rates may cause the disappearance of oscillations by increasing the oxygen dissolution rate which is a direct inhibitor of the BZ reaction [32, 38]. At present, a satisfactory explanation has not been proposed for the stirring effects on the oscillations in a "closed" BZ system. Despite this, it is considered that the effects of oxygen and the effects of stirring have different manifestations in the OCP fluctuation. In a closed BZ system with agitation, the parameters characterizing the oscillations depend on the speed of agitation [38].

### 3.2. Effect of type and size of substrate electrode

Figure 2 compares the OCP recorded using different substrates (Au, Pt, and GC) and sizes (micro- and macro-) of electrodes. The behavior of the OCP shows that the BZ system moves to positive values during the induction period, and then decreases its potential starting the oscillatory regime. During the induction period, changes in the OCP value depend on the type of substrate. In its initial stage, the oscillations display instability and after 10 to 15 min are regularized in both amplitude and period.

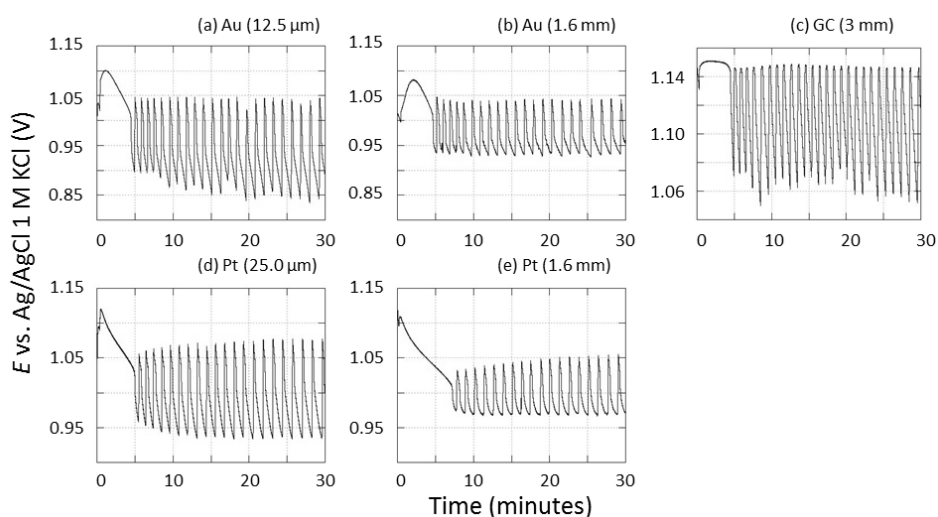


**Figure 2.** Oscillations of the OCP (V) for the BZ reaction recorded on different substrates and sizes (areas) of electrodes: 0.8 M  $\text{H}_2\text{SO}_4$ , 0.10 M MA, 0.08 M  $\text{KBrO}_3$ , and 1 mM  $\text{Ce}(\text{SO}_4)_2$ , at a 375-rpm stirring rate.

The effect of the electrode size (area) in the OCP oscillations can be seen in Au and Pt (Figure 2 a, b, d, e). In both cases, the OCP detected with micro-electrodes ( $d = 12.5 \mu\text{m}$  and  $25.0 \mu\text{m}$ , Au and Pt, respectively) moves rapidly toward more negative values than those observed in the macro-electrode ( $d = 1.6 \text{ mm}$ ). This is due to the smaller area of the micro-electrode which gives a smaller time constant. Furthermore, the micro-dimension allows greater sensitivity to follow concentration variations of the ionic species involved in the BZ reaction in lower solution volumes at the electrode double layer.

As reported in the literature, a micro-electrode can generate more reliable electrochemical signals than a macro-electrode, that is, an electrode of a few millimeters in diameter. For the potentiometric measurements used here, the micro-electrodes have an overall lower time constant (RC) because the smaller area gives rise to a smaller double layer capacitance [39]. In general, higher oscillation amplitude was observed in the OCP when using micro-electrodes (Figure 2) likely due to their faster response.

### 3.3. Characterization of the oscillations using Fast Fourier Transform

Fast Fourier Transform (FFT) is a useful tool for determining the frequencies of stationary and transient signals. Figure 3 shows a Fourier analysis, obtained with GNU Octave, of the oscillation signals of the OCP for BZ reaction recorded at different substrates and size of working electrodes.

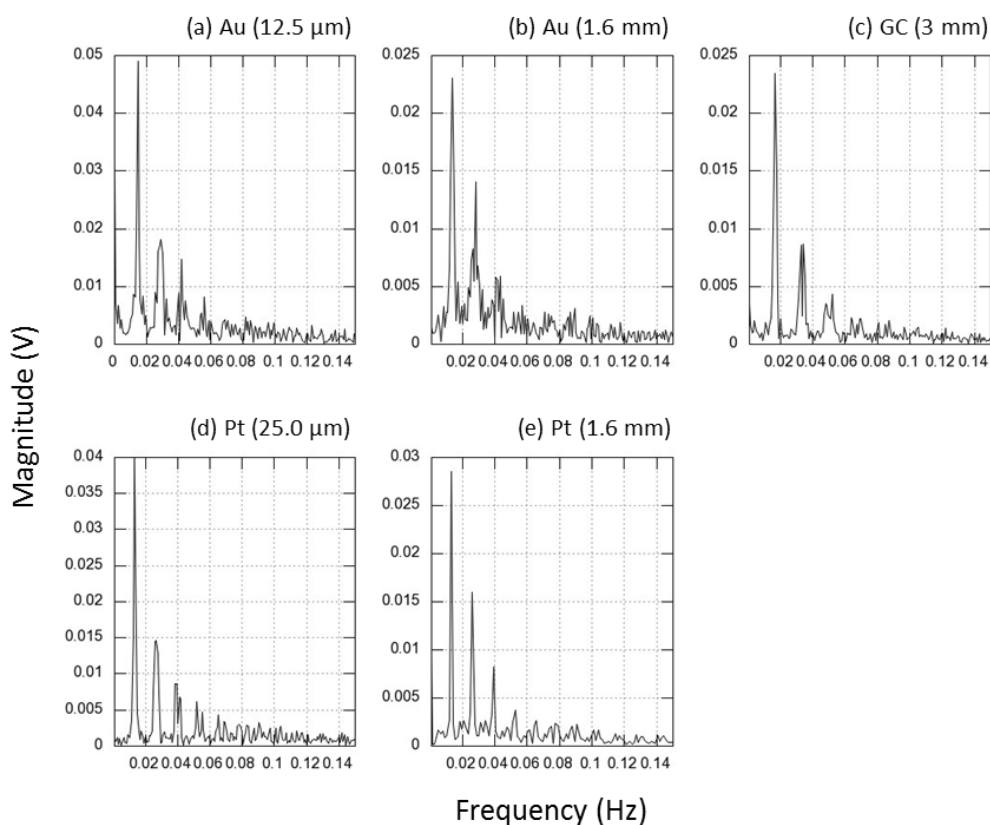


**Figure 3.** Fast Fourier Transform of the OCP oscillations for the BZ reaction, recorded on different substrates and electrode sizes: 0.8 M  $\text{H}_2\text{SO}_4$ , 0.10 M MA, 0.08 M  $\text{KBrO}_3$ , and 1 mM  $\text{Ce}(\text{SO}_4)_2$ , at a 375-rpm stirring rate. Frequency of sampling,  $f_s$ , is  $50 \text{ s}^{-1}$ .

FFT graphs show a fundamental frequency  $f_1$  confirming the periodicity of the phenomena. The lower magnitude peaks ( $f = 2f_1, 3f_1, 4f_1, \dots$ ) correspond to the harmonic components of the Fourier series. The presence of harmonics is due to the non-sinusoidal nature of the signal. When using a sampling frequency  $f_s$  of 50 data/s, the FFT yields symmetrical data around  $\frac{1}{2}$  of the Nyquist frequency of 25 Hz. The fundamental frequency  $f_1$  (mHz) for each electrode is: 14.7 (Au,  $d = 12.5 \mu\text{m}$ ), 13.9 (Au,  $d = 1.6 \text{ mm}$ ), 17.1 (GC,  $d = 3 \text{ mm}$ ), 13.5 (Pt,  $d = 25 \mu\text{m}$ ), and 13.3 (Pt,  $d = 1.6 \text{ mm}$ ).

Our major interest was the OCP oscillatory component; therefore, the baseline of each signal was subtracted to remove the constant component whose transform generates a zero-Hz frequency peak. The data presented indicate higher values for the fundamental frequency when using micro-electrodes (Figure 3 a, d). The fundamental frequency obtained with the macro-GC electrode (Figure 3 c) was higher than those obtained with Au and Pt electrodes, indicating a greater number of oscillations in the BZ system than previously observed with macroelectrodes. In addition, the different components in the FFT for the oscillation of different electrodes also indicate that the materials are sensitive to different electrochemically active species.

### 3.4. Duration and destination of the BZ reaction

In a closed system, the oscillatory regime of the BZ reaction has a finite time. In this study, we followed the evolution in time of the OCP for 18 h using Pt and Au micro-electrodes. As can be observed (Figure 4), the time it takes for the system to achieve the experimental thermodynamic equilibrium depends on the type of electrode substrate. The oscillations suddenly stopped after 9 h on the surface of a Pt micro-electrode ( $25.0 \mu\text{m}$ ) and after 10.2 h on the surface of an Au micro-electrode ( $12.5 \mu\text{m}$ ). In our study, we were not able to obtain OCP data for times higher than one hour when using macro-electrodes, mostly because their greater work area facilitated adhesion of  $\text{CO}_2$  bubbles formed during the BZ reaction that prevented potential data acquisition.

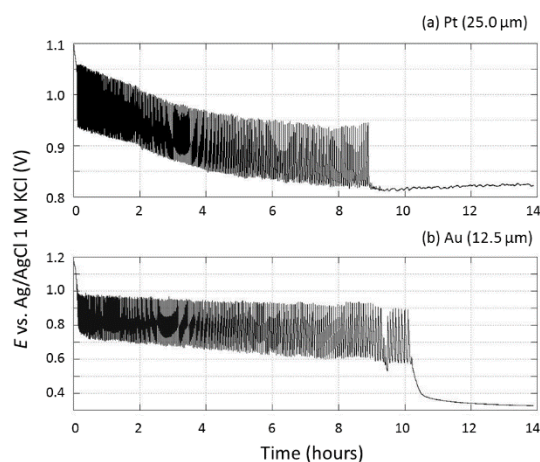
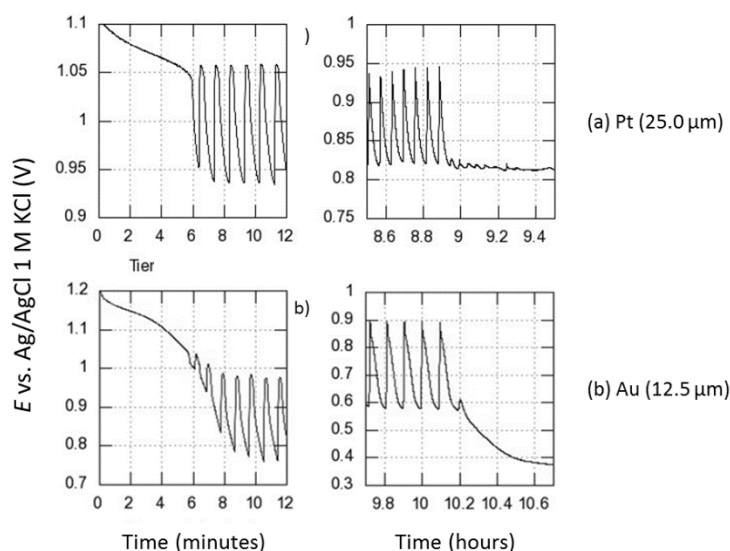


**Figure 4.** OCP oscillations (V) of the BZ reaction registered using a Pt (a) and Au (b) micro-electrode: 0.8 M  $\text{H}_2\text{SO}_4$ , 0.10 M MA, 0.08 M  $\text{KBrO}_3$ , and 1 mM  $\text{Ce}(\text{SO}_4)_2$ , at a 375-rpm stirring rate.

It should be noted the BZ-system characteristic behavior at the oscillations ceases when the two major reagents have been exhausted (bromate and MA). Likewise, the number of oscillations in OCP turned out to be independent of the type of electrode substrate. In the Pt micro-electrode  $274 \pm 4$  oscillations were recorded, whereas in the Au micro-electrode  $272 \pm 3$  oscillations were recorded.

According to Onuma and co-workers [31], three different destinations for the BZ reaction exist, once the oscillations have ceased: (1) Processes with oscillations revival, in which case an interesting and sudden restoration of the oscillator happens with almost the same amplitude as it had before stopping. (2) Processes ending in a reduced steady-state without rebirth of the oscillations, wherein the OCP decreases to a more negative value after the oscillator has stopped. (3) Processes ending in oxidative steady-state without reviving the oscillations, wherein the OCP increases to a more positive value after the oscillations have ceased.

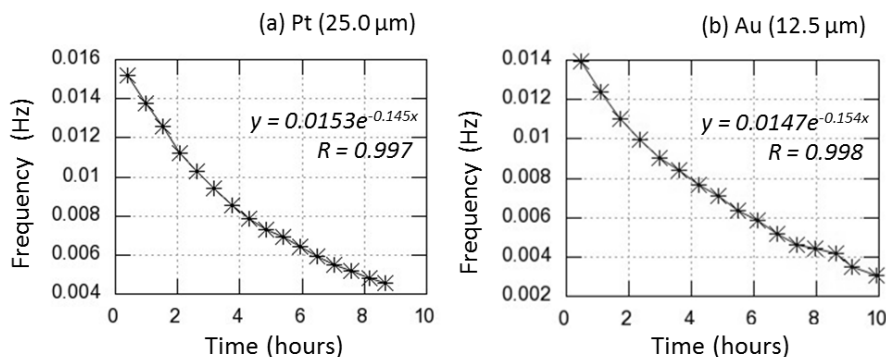
At the end of oscillations, the thermodynamic equilibrium of the BZ system studied (Figure 5) is characterized by a non-oscillatory steady-state with an OCP more negative than its initial value. Furthermore, in the case of Au substrate, the OCP steady-state is 0.4 V more negative than the Pt electrode OCP. Therefore, after the oscillations have ceased, a reduced steady-state prevails. During this state, the solution was colorless, indicating the preponderance of  $\text{Ce}^{+3}$  ions to  $\text{Ce}^{+4}$  ions. The oscillatory regime of the BZ reaction in a closed system before equilibrium possesses a transient behavior. The period and amplitude of the oscillations gradually increases while decreasing the oscillation baseline, that is, there is a negative shift in potential (Figs. 4 and 5).



**Figure 5.** OCP oscillations (V) of the registered BZ reaction using two micro-electrodes: (a) Pt (25.0 μm diam) and (b) Au (12.5 μm diam), showing the beginning of the BZ reaction (left) and the cessation of the oscillations (right): 0.8 M  $\text{H}_2\text{SO}_4$ , 0.10 M MA, 0.08 M  $\text{KBrO}_3$ , and 1 mM  $\text{Ce}(\text{SO}_4)_2$ , at 375-rpm stirring rate.

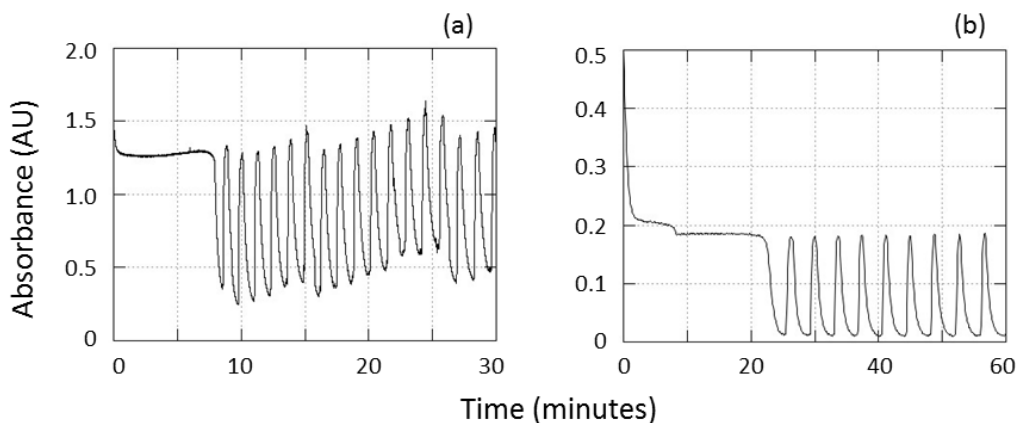
When using FFT analysis for the OCP records using the Pt and Au as micro-electrodes (Figure 4), the falloff of the oscillation frequency can be evaluated for the BZ system. The reduction of the fundamental frequency for the oscillations during the progression of the BZ reaction is presented in

Figure 6. There is a good exponential fit using both electrode substrates. For Pt micro-electrode,  $y = 0.0153\exp(-0.145x)$ ,  $R = 0.997$ ; for Au micro-electrode,  $y = 0.0147\exp(-0.154x)$ ,  $R = 0.998$ . It can be seen that the falloff of the oscillations' fundamental frequency is slightly greater when using an Au micro-electrode (10.87 mHz) rather than a Pt micro-electrode (10.65 mHz). Consequently, the fundamental frequency does not depend largely on the type of substrate.



**Figure 6.** Fall in the fundamental frequency of the oscillations during the course of the BZ reaction registered in micro-electrodes: (a) Pt (25.0  $\mu\text{m}$ ) and (B) Au (12.5  $\mu\text{m}$ ): 0.8 M  $\text{H}_2\text{SO}_4$ , 0.10 M MA, 0.08 M  $\text{KBrO}_3$ , and 1 mM  $\text{Ce}(\text{SO}_4)_2$ , at a 375-rpm stirring rate.

### 3.5. Spectrophotometric analysis of the BZ reaction



**Figure 7.** Reaction profile detected at 217 nm, which is the wavelength proportional to  $\text{Ce}^{+4}$  concentration using (a) an optic fiber probe in a beaker filled with 20 mL of reaction solution at a 375-rpm stirring rate; (b) a cuvette ( $b = 1$  cm) filled with 2 mL of reaction solution (dilution factor of 4, except for the acid) without stirring.

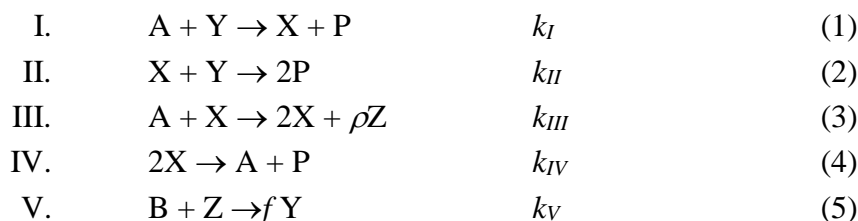
The oscillations recorded during the BZ reaction can be monitored in a variety of forms, from changes in color and pH to changes in potential. In this study, we used a simpler approach to follow chemical oscillations over time by measuring the absorbance with an UV-vis detector. In this qualitative test, it was possible to observe the induction period and the oscillatory profile of the BZ reaction, as a result of changes in the ionic concentration of cerium (Figure 7). The wavelength whose adsorption is proportional to the concentration of  $\text{Ce}^{+4}$ , which represents one of the absorption maxima of 1 mM

Ce(SO<sub>4</sub>)<sub>2</sub> in a 0.8 M H<sub>2</sub>SO<sub>4</sub> solution, was 217 nm. The BZ reaction is sensitive to initial experimental conditions, and although some effect of the incident light on the system may be expected, these have been found to be negligible [31].

The absorbance record over time (Figure 7) was performed using the same geometry and stirring conditions as the previous OCP experiments. While monitoring the absorbance, periodical and irregular oscillations were observed (Figure 7 a), which made clear that the probe disturbs the BZ system, presumptively by easing the CO<sub>2</sub> adherence on the probe's surface. Therefore, we used a conventional spectrophotometer cuvette without stirring (Figure 7 b). It was necessary to dilute the system (1:4) because the CO<sub>2</sub> formation generated light scattering producing measurement errors. In the latter case, periodic oscillations were observed with both regular amplitude and period. Hence, the absorbance data obtained with diluted conditions were used for numeric analysis.

### 3.6. Numerical integration of the BZ reaction in the Oregonator model

Detailed analysis of the BZ reaction is complex due to the large number of phases and chemical species involved. The design of models that preserve the main features of the BZ reaction has been important. One of the most studied is the *Oregonator* (from Oregon and oscillator) first proposed by Field and Noyes at the University of Oregon [30]. The *Oregonator* consists of five stoichiometric steps:



where  $\rho$  is a constant and  $k_{I-IV}$  are constants with known values [24-25]. The constants used for the model are given in Table 1.

**Table 1.** Constants used for the kinetic model of equations (1) – (5).

Kinetic rate constants	Initial concentrations [M]
$k_I = 2.1 \text{ M}^{-1} \text{ s}^{-1}$	[A] = 0.08
$k_{II} = 2 \times 10^9 \text{ M}^{-1} \text{ s}^{-1}$	(A = BrO <sub>3</sub> <sup>-</sup> )
$k_{III} = 1 \times 10^4 \text{ M}^{-1} \text{ s}^{-1}$	<i>Intermediates:</i>
$k_{IV} = 4 \times 10^7 \text{ M}^{-1} \text{ s}^{-1}$	[X] = 0, [Y] = 0,
	[Z] = 0.001
$k_V = 1 \text{ s}^{-1}$ (a)	[P] = 0
	X = HBrO <sub>2</sub> , Y = Br <sup>-</sup> , Z =
	Ce <sup>+4</sup>
	P = 0.5 HOBr, P is treated
	as an inert product

NOTE: All pseudo–first-order constants assume the experimental value  $[H^+] = 1 \text{ M}$  to be constant. (a)  $k_V$  is given an arbitrary value which is treated as constant during the calculation. (after ref [30])

The  $k_V$  value and the stoichiometric factor  $f$  are treated as adjustable parameters, with  $k_V$  usually in the range 0.01–1 and  $f = 1$  for  $\rho = 1$  or  $f = 0.5$  for  $\rho = 2$ . Bromate concentration ( $A$ ) is taken as constant, and the HOBr concentration ( $P$ ) does not appear in the governing kinetic equations [40]. More sophisticated analysis allows  $f$  to fluctuate with the instantaneous concentrations of MA, BrMA, and HOBr.

The underlying dynamics of the *Oregonator* is an activator/inhibitor system containing an autocatalytic step and a negative delayed feedback loop step via  $\text{III} \rightarrow \text{V} \rightarrow \text{II}$  which in turn inhibits the autocatalytic production of  $X$  in step III. These five stages combined in proportion  $\{1, 1, 2, 1, 2\}$  to produce the overall reaction  $A + B + (1 - f)Y \rightarrow 2P + (\rho - 1)Z$ . The variables of the chemical species involved in the BZ reaction (equations 1-5) are [41]:  $\text{BrO}_3^-$  ( $A$ ); MA ( $B$ ); HOBr ( $P$ );  $\text{HBrO}_2$  ( $X$ );  $\text{Br}^-$  ( $Y$ ); and  $\text{Ce}^{+4}$  ( $Z$ ). Field employed this model to discuss the excitability of a stable steady-state to small, but finite, perturbations and explained successfully the period irregularities approaching the end of the chemical oscillations [42].

In this study, the numerical integration of the Field–Noyes equations [1, 43] was performed using the experimental concentration values of the chemical species involved in the BZ reaction and the rate constants reported in the literature [24-25]. In the numerical integration, or *Oregonator*, the concentrations were transformed to dimensionless variables,  $X$ ,  $Y$ , and  $Z$ . Nevertheless, these variables still represent the chemical concentration of bromous acid, bromide ion, and ceric ion, respectively.

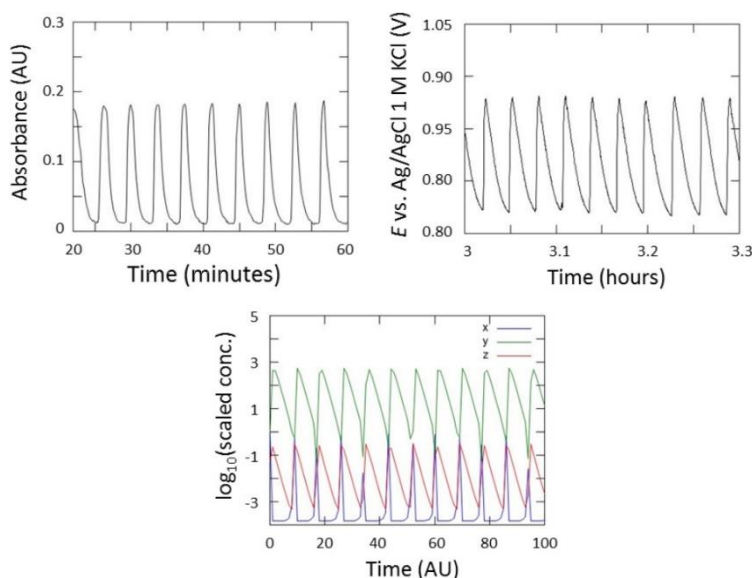


**Figure 8.** *Top:* Absorbance oscillations proportional to  $\text{Ce}^{+4}$  and OCP oscillations obtained experimentally (Figure 7b and 4a). *Bottom:* Numerical integration of the Field–Noyes equations (*Oregonator*) for the experimental parameters used in this study. Variables  $X$ ,  $Y$ , and  $Z$  represent bromous acid, bromide ion, and  $\text{Ce}^{+4}$ , respectively. The initial conditions for the numerical resolution were  $x_0 = y_0 = 0$ ,  $z_0 = 0.001$ . Major species:  $A = \text{KBrO}_3 = 0.08 \text{ M}$ ,  $B = \text{MA} = 0.08 \text{ M}$ .

These values correspond to the region of instability of the system based on the diagrams of the model available in the literature. For example, in the *Oregonator* model used in this paper (ref [30], Figure 6) we are clearly in the unstable region. We analyze this bifurcation diagram based on the initial experimental concentrations used here and with the kinetic parameters used in the simulations that reproduce qualitatively the experimental observations. Under our specific conditions,  $k_V = 1$  (reaction V) and  $f = 1$ , where  $f$  is the so-called stoichiometric coefficient of reaction V. The analysis is based on the previously reported parameters and constraints for the *Oregonator* model used in this work (reference [30]). The parameters and conditions follow:

$$s = \sqrt{\frac{k_{III} B}{k_I A}} \tag{6}$$

$$w = \frac{k_V}{\sqrt{k_I k_{III} AB}} \tag{7}$$

$$q = \frac{2k_I k_{IV} A}{k_{II} k_{III} B} \tag{8}$$

$$\alpha_{ss} = \frac{(1 - f - q) + [(q + f - 1)^2 + 4(f + 1)q]^{1/2}}{2q} \tag{9}$$

$$\eta_{ss} = \frac{f\alpha_{ss}}{1 + \alpha_{ss}} \tag{10}$$

$$a = s(1 - 2\alpha_{ss}q) - \eta_{ss} \tag{11}$$

$$b = s(1 - \alpha_{ss}) \tag{12}$$

$$c = (1 + \alpha_{ss}) / s \tag{13}$$

$$d = -\eta_{ss} / s \tag{14}$$

The constraints for oscillatory behavior were derived from analytical solutions of the simplified *Oregonator* model given in reference 27. The conditions for oscillations are given by equation 15, for the kinetic parameters for which  $Q < 0$ , which are shown in Figure 9. The graph is drawn based on the condition that  $Q = 0$  for a set of  $k_V$  and  $f$  values in equation 15. The  $k_V$  and  $f$  values for which  $Q = 0$  are the lines in Figure 9 for different experimental concentrations while the area below the curves represents the  $k_V$  and  $f$  values that are consistent with oscillatory behavior. These stability criteria were derived in reference [30], Figure 6 therein.

$$Q = -[ac + bd + (a - c)w] < 0 \tag{15}$$

where the parameters are defined above, eq. (6–14). The lines in Figure 9 represent the solutions for  $Q = 0$  (eq.15), with the regions under the curve corresponding to the oscillatory region. We show the results for  $Q = 0$  for our initial concentrations (—), for  $A = B = 0.08$  M and with  $k_{III} = 1 \times 10^4$  M<sup>-1</sup> s<sup>-1</sup>. For comparison, the graph also shows the solution for the conditions in the original reference (- - - for  $A = B = 0.06$ ,  $k_{III} = 8 \times 10^3$  M<sup>-1</sup> s<sup>-1</sup>) [30], with our proposed starting point marked (x)  $k_V = 1$  s<sup>-1</sup>,  $f = 1$ . Note that the difference in concentrations and the larger rate constant  $k_{III}$  used in the simulations predicts oscillations for a larger range of  $k_V$  values, in other words, the model indicates that the observation of oscillations is consistent with  $k_V < 745$  s<sup>-1</sup> ( $k_V$  maximum in Figure 9). We point out that different models exist in the literature because the kinetics in equations (I) – (V) can be treated as pseudo-first-order-like in the work presented here, or an alternate model could include explicit second-order rate constants. The

mechanism can also be re-written with different stoichiometric coefficients, especially in the case of the redox cycle in equation V, such as in the model given by Tyson [44] based on a review of the *Oregonator*. In any case, the predictions of these models are qualitative and our experimentally observed oscillations are consistent with previous kinetic studies of the *Oregonator* system: we observe oscillations because our experimental conditions correspond to the unstable region of the available stability diagrams (e.g., refs [30, 44]), such as the one in Figure 9. While a study of the proposed mathematical models is outside the scope of this paper, we focus on the use of the *Oregonator* [30] to discuss our observations from the qualitative reconstruction of the observed oscillations.

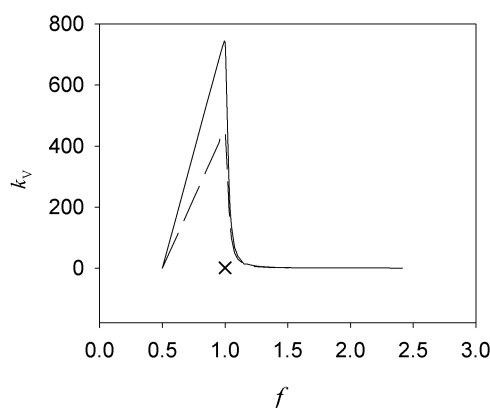


**Figure 9.** Instability region of the *Oregonator* steady state. The lines indicate the values for  $f$  and  $k_v$  for which  $Q = 0$  (eq. 15), with the area under the lines corresponding to oscillations. (—)  $A = B = 0.08$  M and with  $k_{III} = 1 \times 10^4$   $M^{-1} s^{-1}$ , used in this work; (- - -) for  $A = B = 0.06$ ,  $k_{III} = 8 \times 10^3$   $M^{-1} s^{-1}$  as in ref 27. (x) marks the initial experimental conditions proposed here, assuming  $k_v = 1$   $s^{-1}$ ,  $f = 1$ ; these values reproduce qualitatively the oscillations as shown in Figure 8.

To summarize, the chemical oscillations of each intermediary ( $X$ ,  $Y$ , and  $Z$ ) were reproduced and the values used for the simulations are consistent with the predictions of the *Oregonator* that oscillations will be present (Figure 9) [30]. Figure 8 shows the dynamic behavior of the calculated concentration of  $Ce^{+4}$ , ( $Z$  in the numeric solutions), that is comparable to the absorbance and electrochemical OCP oscillations obtained experimentally. We must remember that concentration variations occur exclusively for some intermediary species; however, the main reactants (malonic acid and bromate ion) decrease slowly but continuously during the reaction process (oscillatory phase). Hence, the reaction flows directly toward the path that decrease the free energy: no oscillations happen in the overall reaction direction, which is always moving inexorably toward the equilibrium state [40, 45].

#### 4. CONCLUSIONS

The Belousov-Zhabotinskii (BZ) reaction was studied in presence of  $Ce^{+4}/Ce^{+3}$  catalyst on different substrates of Pt, Au, and glassy carbon micro- and macro-electrodes, applying different stirring rates to the system comprising of sulfuric acid, malonic acid, bromate ion, and cerium ion. The open circuit potential (OCP) in the closed BZ system exhibits a non-oscillatory induction period, followed by

an oscillatory phase. Both stages depend on experimental conditions, such as substrate type, size (area) of electrode, and stirring. With each oscillation, the solution's color alternated between colorless and yellow according to the catalyst oxidation state, reduced ( $\text{Ce}^{+3}$ ) or oxidized ( $\text{Ce}^{+4}$ ), respectively.

The OCP oscillations registered by micro-electrodes (12.5- and 25.0- $\mu\text{m}$  in diameter) display higher frequency and amplitude and overall more stable oscillations compared to macro-electrodes. We can assign these findings to the smaller electrode dimensions which confer a lower time constant, thus improving the detection limits of the OCP value. With increasing stirring rate for the BZ electrolyte (from 0 rpm to 1200 rpm), the oscillation amplitude augments (from 77 to 153 mV) and the period diminishes (from 1,273 to 1,112 minutes). Furthermore, a time delay exists in the induction period.

OCP oscillations cease when the BZ system relaxes towards thermodynamic equilibrium characterized by a steady reduced state (more negative OCP values). The time required to reach this state depends on the type of micro-electrode substrate: 9 h for Pt, and 10.2 h for Au. However, the number of oscillations is independent of the substrate and is about 272 and 274, for Au and Pt, respectively. The fixed number of oscillations with different oscillation times, and the observation that the FFT spectrum as well as the OCP offset is a function of the electrode material indicates that the Au, C, and Pt electrodes are sensitive to different redox species that oscillate with different characteristic times, but interestingly, have the same number of cycles in our experimental conditions.

The falloff of the fundamental frequency for the oscillations in the BZ system using two different micro-electrodes (Pt and Au) proved to fit exponentially. The frequency drop does not depend greatly on the type of substrate: in Au micro-electrode resulted in 10.87 mHz, while the Pt micro-electrode resulted in 10.65 mHz. Using the wavelength adsorbed by the catalyst  $\text{Ce}^{+4}$ , we could track the BZ reaction fundamental oscillations and these were reproduced numerically. Chemical oscillations for the Ce catalyst concentration were successfully reproduced using a numerical integration provided by the *Oregonator*. The dynamical behavior and oscillatory profile were similar to that obtained experimentally. Overall, the OCP oscillations represent the fundamental frequency of the BZ reaction, although they also carry information of redox species that have different affinities to the electrode materials. These redox processes are the subject of our current investigation and will be presented in due time.

#### ACKNOWLEDGMENTS

L. Veleza and G. Perez thank CINVESTAV-Merida. M. A. Alpuche-Aviles acknowledges financial support from National Science Foundation, Career Award No CHE-1255387, and NSF MRI-1726897 and the University of Nevada, Reno, Office of the Provost through an International Activity Grant. We also acknowledge Salvador Gutierrez-Portocarrero for the SEM image. M.A. Gracia-Nava thanks Mexican CONACYT scholarship provided during his study in the Physical Chemistry program at CINVESTAV-Merida and the Beca Mixta that funded his stay at UNR.

#### References

1. S.K. Scott, *Oscillations, Waves and Chaos in Chemical Kinetics*. Oxford University Press, (1994) New York.
2. A.F. Taylor, M.R. Tinsley, F. Wang, Z. Huang and K. Showalter, *Science*, 323 (2009) 614.

3. T. Bánsági, V.K. Vanag and I.R. Epstein, *Science*, 331 (2011) 1309.
4. Y. Jia and I.Z. Kiss, *J. Phys. Chem. C*, 116 (2012) 19290.
5. J.L. Hudson and T.T. Tsotsis, *Chem. Eng. Sci.*, 49 (1994) 1493.
6. M.T.M. Koper, *Adv. Chem. Phys.*, 92 (1996) 161.
7. K. Krischer, B.E. Conway, O.M. Bockris and R.E. White, *Modern Aspects of Electrochemistry*. (1999) Vol. 32.
8. K. Krischer, H. Varela, W. Vielstich, A. Lamm and H.A. Gasteiger, *Handbook of Fuel Cells—Fundamentals, Technology and Applications*. (2003) Vol. 2, 679.
9. I.R. Epstein, *Physica D*, 51 (1991) 152.
10. A.M. Zhabotinsky, *Chaos*, 1 (1991) 379.
11. F. Blaffart, Q. Van Overmeere, F. Van Wouwerghem and J. Proost, *J. Electrochem. Soc.*, 161 (2014) H874.
12. R. Nagao, W. Zou, J. Kurths and I.Z. Kiss, *Chaos*, 26 (2016) 094808/1.
13. S. Bozdech, K. Krischer, D.A. Crespo-Yapur, E. Savinova and A. Bonnefont, *Faraday Discussions*, (2016).
14. A.S. Mikhailov and G. Ertl, *ChemPhysChem*, 10 (2009) 86.
15. A.M. Zhabotinsky, *Biofizika*, 9 (1964) 304.
16. A.N. Zaikin and A.M. Zhabotinsky, *Nature*, 225 (1970) 535.
17. M. Seipel, M. Zierhut and A.F. Münster, *ChemPhysChem*, 2 (2001) 613.
18. R.J. Dylla and B.A. Korgel, *ChemPhysChem*, 2 (2001) 62.
19. D.A. López-Sauri, L. Veleza and G. Pérez, *Int. J. Electrochem. Sci.*, 9 (2014) 1102.
20. W. Uddin, G. Hu, L. Hu, Z. Fang, Y. Zhang and J. Song, *Int. J. Electrochem. Sci.*, 12 (2017) 178.
21. W. Uddin, G. Hu, L. Hu, Y. Hu, Z. Fang, S. Ullah, X. Sun, X. Shen and J. Song, *Int. J. Electrochem. Sci.*, 12 (2017) 4193.
22. P.V. Coveney, *Nature*, 333 (1988) 409.
23. I. Prigogine and R. Balescu, *Bull. Cl. Sci., Acad. R. Belg.*, 42 (1956) 256.
24. R.J. Field, E. Koros and R.M. Noyes, *J. Am. Chem. Soc.*, 94 (1972) 8649.
25. L. Gyorgyi, T. Turanyi and R.J. Field, *J. Phys. Chem.*, 94 (1990) 7162.
26. O. Benini, R. Cervellati and P. Fetto, *J. Chem. Educ.*, 73 (1996) 865.
27. N.A. Kudryashov and A.S. Zakharchenko, *Chaos, Solitons Fractals*, 65 (2014) 111.
28. M. Mazzotti, G. Serrvalle and M. Morbidelli, *Chem. Eng. Sci.*, 49 (1994) 681.
29. H. Brandtstädter, M. Braune, I. Schebesch and H. Engel, *Chem. Phys. Lett.*, 323 (2000) 145.
30. R.J. Field and R.M. Noyes, *J. Chem. Phys.*, 60 (1974) 1877.
31. H. Onuma, A. Okubo, M. Yokokawa, M. Endo, A. Kurihashi and H. Sawahata, *J. Phys. Chem. A*, 115 (2011) 14137.
32. J.A. Pojman, R. Craven and D.C. Leard, *J. Chem. Educ.*, 71 (1994) 84.
33. R.M. Wightman and D.O. Wipf, *Voltammetry at Ultramicroelectrodes*. In *Electroanal. Chem.*, Bard, A. J., Ed. (1989) Vol. 15, pp 267.
34. J.E. Eaton, D. Bateman and S. Hauberg *GNU Octave*, 3.0.1; CreateSpace Independent Publishing Plattform (2009).
35. C.D. Baird, H.B. Reynolds and M.A. Crawford, *J. Chem. Educ.*, 88 (2011) 960.
36. I.R. Epstein, *Physica D*, 7 (1983) 47.
37. A.T. Winfree, *Science*, 175 (1972) 634.
38. P. Ševčíky and Ľ. Adamčíková, *Chem. Phys. Lett.*, 146 (1988) 419.
39. A.J. Bard and L.R. Faulkner, *Electrochemical methods: fundamentals and applications*. 2<sup>nd</sup> ed.; John Wiley & Sons, (2000) New York, 471.
40. P. Atkins and J. de Paula, In *Physical Chemistry*, 7th ed.; W. H. Freeman and Company, (2012) New York, 914.
41. W.R. Derric, *Mathematics of chaos in perturbed oscillators*. In *Chaos in Chemistry and Biochemistry*, Field, R. J.; Györgyi, L., Eds. World Scientific Publishing Co., (1993) Singapore,

- 1.
42. R.J. Field, *J. Chem. Phys.*, 63 (1975) 2289.
43. R.J. Field and R.M. Noyes, *J. Chem. Phys.*, 60 (1974) 1877.
44. J.J. Tyson, *J. Chem. Phys.*, 66 (1977) 905.
45. J.I. Steinfeld, J.S. Francisco and W.L. Hase, *Chemical kinetics and dynamics*. 2<sup>nd</sup> ed.; Prentice Hall, (1998) New Jersey, 518.

© 2019 The Authors. Published by ESG ([www.electrochemsci.org](http://www.electrochemsci.org)). This article is an open access article distributed under the terms and conditions of the Creative Commons Attribution license (<http://creativecommons.org/licenses/by/4.0/>).